JAIST Repository
https://dspace.jaist.ac.jp/

Title	Raman spectral analysis of Si films solid-phase-crystallized on glass substrates using pulse laser with crystallization-induction layers of yttria-stabilized zirconia
Author(s)	Mai, Thi Kieu Lien; Horita, Susumu
Citation	Japanese Journal of Applied Physics, 53(3S1): 03CB01-1-03CB01-7
Issue Date	2014-02-06
Type	Journal Article
Text version	author
URL	http://hdl.handle.net/10119/11938
Rights	This is the author's version of the work. It is posted here by permission of The Japan Society of Applied Physics. Copyright (C) 2014 The Japan Society of Applied Physics. Mai Thi Kieu Lien and Susumu Horita, Japanese Journal of Applied Physics, 53(3S1), 2014, 03CB01-1-03CB01-7. http://dx.doi.org/10.7567/JJAP.53.03CB01
Description	

Japan Advanced Institute of Science and Technology

Raman spectral analysis of Si films solid-phase-crystallized on glass substrates using pulse laser with crystallization-induction layers of yttria-stabilized zirconia

Mai Thi Kieu Lien and Susumu Horita

School of Materials Science, Japan Advanced Institute of Science and Technology, 1-1 Asahidai, Nomi, Ishikawa 923 – 1292, Japan

E-mail: Mai Thi Kieu Lien (mai.lien@jaist.ac.jp); Susumu Horita (horita@jaist.ac.jp)

The solid-phase crystallization of amorphous Si films with/without a crystallization-induction (CI) layer of yttria-stabilized zirconia (YSZ) was performed using a Nd:YAG pulse laser. We investigated the crystallinity of the Si films by Raman spectroscopy. It was found that, at the same crystalline fraction, the FWHM of the c-Si peak for Si/YSZ/glass was smaller than that for Si/glass. The result is considered owing to the CI effect of the YSZ layer. This was confirmed by scanning electron microscopy observation, which showed that the grain size of Si on YSZ layers was more uniform than that on glass substrates. On the other hand, at a lower beam energy, the crystalline quality of the Si films was found to be better although the increase in the crystallization rate with the pulse number N is lower. On the basis of the above results, the crystallization model of an a-Si film on a YSZ layer is speculated.

1. Introduction

Semiconductor thin films on non-heat-resistant and inexpensive insulating substrates made of glass or plastic have received much interest as materials for actual devices, e.g., thin-film transistors (TFTs), solar cells, and sensors[1-4]. In order to improve the properties of TFTs such as mobility and reliability, and to lower production costs to meet application needs, a large number of studies of TFT channel materials using oxide[5-7], organic[8, 9], and crystallized silicon (c-Si)[10, 11] have been carried out extensively. Among these materials, polycrystalline silicon (poly-Si) TFTs have great advantages of higher stability or reliability and higher mobility. Since the demands for the application of poly-Si TFTs include low cost and high performance, several methods have been proposed[12-30], such as the solid phase crystallization (SPC) method[12-16], metal-induced crystallization (MIC) method[17-20], metal-induced lateral crystallization (MILC) method[21-24], and pulse laser annealing (PLA) method[25-28]. For the SPC method, the fabricated poly-Si film has a smooth surface and a uniform grain size. However, it has drawbacks of high process temperature and long annealing time. The MIC and MILC methods can solve the problems of the SPC method. However, the disadvantage of these methods is the remnant metal that becomes a leakage current source in poly-Si TFTs. The PLA method can reduce crystallization temperature to room temperature, and its melting-crystallized films have large grains with high mobility. However, melting-crystallized films have the drawbacks of high film surface roughness and nonuniformity of grain size, which lead to nonuniform device performance.

Therefore, in order to obtain a poly-Si film with uniform electrical properties in terms of both short time and low temperature, we have proposed a crystallization-induction (CI) layer method using yttria-stabilized zirconia [$(ZrO_2)_{1-x}(Y_2O_3)_x$:YSZ] as the CI material[31, 32].

In this method, an amorphous Si (a-Si) film is deposited on a YSZ layer that covers surface of a glass substrate. Since YSZ has a small lattice mismatch of ~5% and the same cubic crystal structure as Si, it can be expected that the obtained poly-Si film will have uniform grain size and crystallographic information, owing to the crystallographic information of the YSZ layer. Actually, we have reported that, in the CI layer method, the crystallization of a Si film directly deposited on a YSZ layer occurs at a substrate temperature of 320 ^{o}C, which is lower than that on a glass substrate without a YSZ layer by more than 100 ^{o}C [32]. However, the deposition temperature >300 ^{o}C is not low enough for non-heat-resistant device applications such as flexible displays with a plastic substrate, and the surface of the directly deposited poly-Si film is generally much rougher than that of SPC poly-Si films. Therefore, for the reduction in fabrication temperature and surface roughness of crystallized Si films, we tried to crystallize an a-Si film in the solid phase by the PLA method at room temperature. The combination of the CI layer and SPC-PLA methods is thought to have high potential not only for eliminating the drawback of the melting-PLA method, but also for satisfying the demands for the application of poly-Si TFTs. In the investigation, we focused on the CI effect of the YSZ layer on the SPC of a-Si films, compared with the SPC without YSZ layers. The crystallized Si films were measured mainly by Raman spectroscopy, and the crystalline fraction X_c and the FWHM and position of the c-Si peak were evaluated. We can roughly estimate crystalline quality from the FWHM of the c-Si peak and film stress from the peak position. Also, Secco-etched Si films were observed by scanning electron microscopy (SEM) for comparison with the films observed by Raman spectral analysis.

In this paper, we show the energy density and pulse number dependences of X_c, and the FWHM and position of the c-Si peak for crystallized Si films on YSZ layers and glass substrates, including SEM images of the films. Results are then discussed and a crystallization model of an a-Si film on a YSZ layer is speculated and compared with that of an a-Si film on a glass substrate.

2. Experimental procedure

A fused quartz glass substrate (1×2 cm^2) is chemically cleaned before the deposition of a YSZ CI layer at a substrate temperature of 50 ^{o}C by reactive magnetron sputtering. Ar and O_2 are used as the sputtering and reactive gases, respectively, with a sputtering pressure of ~6.5 mTorr[33]. Then, an a-Si film is deposited on a YSZ/glass substrate by the e-beam evaporation method at 300 ^{o}C. For comparison, a-Si films are deposited directly on glass substrates without a YSZ layer. Subsequently, the crystallization of a-Si films is performed by PLA in N_2 ambient. A Q-switched Nd:YAG laser (λ = 532 nm) is used for annealing with a repetition frequency of 10 Hz, a pulse duration of 6 − 7 ns, and a beam diameter of ~4 mm. The laser system setup for annealing is shown in Fig. 1. The laser energy density E and the pulse number N are 20 − 160 mJ/cm^2 and 10 − 300, respectively. An a-Si film is irradiated normal to its surface by an incident beam with a beam energy adjusted by an attenuator. Laser beam patterns are taken for each beam power by a CCD camera and analyzed for the estimation of the energy density distribution. The crystalline property of the deposited YSZ layer is estimated by X-ray diffraction (XRD) and *in situ* reflected high-energy electron diffraction (RHEED) measurements. The crystallization degree of Si films is estimated by Raman spectroscopy. In this work, transverse optical phonon (TO) mode spectra in the Raman spectrum measured in each Si film were deconvoluted into three

peaks: a crystalline peak (wave number of 514 − 520 cm^{-1}), a microcrystalline or intermediate peak (503 − 510 cm^{-1}), and an amorphous peak (470 − 490 cm^{-1}). The crystalline fraction X_c and the microcrystalline fraction X_μ are determined by $X_c = (I_\mu + I_c)/(I_\mu + I_c + I_a)$ and $X_\mu = I_\mu/(I_\mu + I_c + I_a)$, respectively, where I_c, I_μ, and I_a are the integrated intensities of the c-Si, microcrystalline silicon (μ-Si), and a-Si peaks, respectively[34]. The analyzed data such as X_c, peak FWHM, and peak position are shown as averages whose error bars indicate the upper and lower values among three measurements at the same point. Grains of poly-Si films are observed by SEM after Secco-etching.

3. Results

Figure 2 shows the XRD and RHEED patterns of the 60-nm-thick YSZ layer deposited on a quartz substrate. It can be seen from the XRD pattern that the deposited YSZ layer has a preferential orientation of (111). Moreover, a spotty pattern can be observed from the RHEED measurement, which indicates a highly oriented film surface. The YSZ layer is found to be uniaxially (111)-oriented because the observed RHEED pattern does not change with rotation along the normal axis of the sample surface, which is in good agreement with the XRD pattern[32, 35].

Figure 3 shows the Raman spectra of the Si films deposited on the YSZ/glass and glass substrates at energy densities E of (a) 29 – 31 and (b) 104 – 106 mJ/cm^2 with $N = 300$. In Fig. 3(b), the spectra of Si/YSZ/glass and Si/glass are shown in the inset for comparison. The dotted lines in the large spectra of Si/YSZ/glass are the decomposed components of the three TO mode peaks, the longitudinal optical (LO) mode peak at 380 ± 20 cm^{-1}, the longitudinal acoustic (LA) mode peak at 300 ± 20 cm^{-1}, and three peaks corresponding to the glass substrate (~490, ~450, and ~180 cm^{-1}); the solid line is their sum, shown as an

example of deconvolution. At a low E of 29 – 31 mJ/cm^2 [Fig. 3(a)], we observe broad and large peaks at ~480 cm^{-1} corresponding to an a-Si phase accompanied by very small c-Si peaks at ~517 cm^{-1} for both Si/glass and Si/YSZ/glass. This suggests that the crystallization of Si films starts at approximately this energy density. At a high E of 104 – 106 mJ/cm^2, the Raman spectra in Fig. 3(b) show high and sharp c-Si peaks at ~515 cm^{-1} with small a-Si peaks, which indicate that a small fraction of a-Si phase still remains. At approximately this energy density, it seems that the crystallization process is almost complete. It can also be seen that the c-Si peaks of Si/glass are slightly higher than those of Si/YSZ/glass at both energy densities.

Figure 4 shows the dependence of the crystalline fraction X_c on laser energy density with N = 300. It can be seen from this figure that X_c increases monotonically with E for both Si/glass and Si/YSZ/glass. At $E \geq 105$ and 110 mJ/cm^2 for Si/glass and Si/YSZ/glass, respectively, the Si films begin to melt, and X_c becomes nearly saturated at a high value. It is considered that, in the low-E region, Si films do not receive sufficient thermal energy for complete amorphous to crystalline phase transformation. Therefore, most of the films are in the amorphous phase. Then, with increasing E, more new nuclei are formed and the crystallization area extends, causing X_c to increase. The X_c's of the Si films on the glass substrates are higher, indicating faster crystallization of these films than of those on the YSZ layers at the same energy density. This is due to the difference in optical absorption of an a-Si film between the Si/glass and Si/YSZ cases. This difference also leads to a difference in the critical E for the melting of Si/glass from that of Si/YSZ/glass, as shown in Fig. 4. The broken blue line in this figure is the curve redrawn with the corrected E for Si/YSZ/glass, considering the difference in optical absorption. The horizontal energy

density E is reduced by 18.5% or the whole curve is shifted along the negative E direction by $\Delta E = 0.185E$. Details will be discussed later with the results of the theoretical optical analysis.

Figures 5(a) and 5(b) show the energy density E dependences of the microcrystalline fraction X_μ and the FWHM of the c-Si peak, respectively. It can be seen from Fig. 5(a) that X_μ initially increases with E and decreases gradually after $E \approx 45 \sim 55$ mJ/cm^2. Since, in the low-E region, most of the Si films are in the amorphous phase, X_μ increases with E. However, after passing a maximum value, X_μ decreases with increasing E probably because the crystal Si-Si bond network extends with higher E or higher heating so that grain size becomes larger. It should be noted that X_μ of Si/YSZ/glass is slightly lower than that of Si/glass. This may indicate that the amount of small grains or micrograins is smaller in the former than in the latter.

In Fig. 5(b), the FWHM of the c-Si peak varies from 4 to 10.5, with increasing E in both Si/glass and Si/YSZ/glass in the SPC regime (i.e., $E < 105$ and 110 mJ/cm^2 for Si/glass and Si/YSZ/glass, respectively). However, near/in the melting regime (i.e., $E \geq 105$ and 110 mJ/cm^2 for Si/glass and Si/YSZ/glass, respectively), the opposite tendency occurs. The increase in FWHM with E in the SPC regime can be explained by the increase in the defect density inside and outside of the grains owing to the rapid crystallization and impingement of grains grown in an inhomogeneous direction[36, 37]. In contrast, near/in the melting regime of E, defects inside and outside of the grains are removed and reduced in number by a higher temperature or a melting process. Moreover, the good lattice realignment of Si atoms in the melting regime makes films more homogeneous. Also, as a whole, it can be seen that the FWHMs of the c-Si peaks for Si/YSZ/glass are smaller than those for Si/glass, which is

similar to the result in Fig. 5(a). Since FWHM is taken as one of the indicators of the crystalline quality of c-Si grains, the crystalline quality of the Si films on the YSZ layers is apparently better than that on the glass substrates. This will also be discussed later in detail.

Figures 6(a) and 6(b) show SEM images of the Secco-etched SPC Si films on glass and YSZ/glass, respectively, where the annealing conditions are $E = 60 - 80$ mJ/cm^2 and $N = 300$. The grain size is roughly about 20 nm for the Si films on both the YSZ layer and the glass substrate. Carefully observing some areas in the Si/glass sample of Fig. 6(a), we can find a large difference in grain size or nonuniform grains. For example, in the left-hand and right-hand circles, smaller and larger grains exist, respectively. This is probably due to the random nucleation of Si on the glass substrate. In contrast, on the YSZ layer, the grain sizes become relatively uniform, as shown in Fig. 6(b). This is probably because, owing to the CI effect of the YSZ layer, the random nucleation and crystallization of the Si film are reduced more on the YSZ layer than on the glass substrate. Therefore, it can be considered that crystallization with uniform grain size because of the presence of the YSZ layer, may result in smaller FWHM or better crystalline quality of crystallized Si films, than in the Si films on glass.

Figures 7(a) and 7(b) show the dependences of the crystalline fraction X_c and the FWHM of the c-Si peak, respectively, on the pulse number N, where energy density is a parameter. It can be seen from Fig. 7(a) that the X_c of Si films increases with N because increasing N increases annealing time substantially, which enhances the crystallization of Si films. It is well known that, for bulk nucleation, the initial crystalline fraction depends on annealing time with the power of 4, under the assumptions that nucleation occurs randomly at a constant rate and that crystallization proceeds isotropically in direction and linearly in

time[38]. Therefore, we can say that the rapid increase in and saturation tendency of X_c with a small N at a high E indicates bulk nucleation and growth. It can also be seen that the X_c's of the Si films on YSZ/glass are lower than those on the glass substrates, in general.

In Fig. 7(b), at a low $E = 29 - 31$ mJ/cm^2, the FWHMs are small and almost the same for all the pulse numbers except $N = 50$ for Si/YSZ/glass. This indicates that annealing with a small E enables crystallization that retains relatively good quality with low defect density. However, by increasing E within the SPC regime, the FWHM becomes larger and increases slightly with N. The increase in FWHM with E is due to the increase in defect density or the degraded crystalline quality, as mentioned earlier in Fig. 5(b). Since the crystallization rate is very high owing to the high E, sudden impingement of grains may promote defect generation not only in the grain boundary region, but also inside grains. Furthermore, it is notable that, at the same N, the FWHMs for Si/YSZ/glass are smaller than those for Si/glass, as in Fig. 5.

In the above results, we compare the FWHMs of the c-Si peak of the Si/YSZ/glass and Si/glass samples at the same energy density. Considering that the crystalline defect region extends with increasing X_c, which is determined not only by E or N but also by the sample structure, i.e., with/without a YSZ layer, we can say that the actual main factor affecting FWHM is not E but X_c. Therefore, as a function of X_c, we check the behaviors of the FWHM and position of the c-Si peak, which are measures of crystalline quality and film stress, respectively. Figure 8 shows the dependences of the FWHM and position of the c-Si peak on X_c with $N = 300$ for Si/YSZ/glass and Si/glass. In this figure, every set of two data points with the same E is enclosed together by one solid circle. The critical X_c's for melting are almost the same for both Si/YSZ/glass and Si/glass. From this figure, it can be seen that

the FWHMs for both Si films increase with X_c up to ~ 60%, then decrease beyond it. Also, at $X_c \geq 30\%$, it can be seen that the FWHMs for Si/YSZ/glass are smaller than those for Si/glass. The differences between them are clearly larger than the measurement error bars. Therefore, it can be concluded that the crystalline quality of the SPC Si film on the YSZ layer is essentially better than that on the glass substrate.

Also, it can be seen from Fig. 8 that the c-Si peak positions in both cases are nearly the same at identified X_c and in the range from 514.5 to 517.4 cm^{-1}, which is lower than the peak position of single-crystalline Si (520 cm^{-1}). This indicates that the Si films exhibit tensile stress on both the YSZ layer and the glass substrate, and that the YSZ layer does not serve as a strain buffer layer. Therefore, it can be considered that the small FWHM of the Si/YSZ/glass is not related to film stress. Generally, tensile stress in a crystallized Si film on a glass substrate can be explained by the difference between the thermal expansion coefficients (TECs) of Si and glass (quartz), which are $2.8 \times 10^{-6}/^{o}C$ and $0.5 \times 10^{-6}/^{o}C$[39], respectively. Since the TEC of Si is much larger than that of glass and the crystallization or atomic arrangement temperature is higher, e.g., the melting temperature, the crystallized Si films at room temperature suffer from tensile stress[28, 36, 37, 40]. However, in our case, since the TEC of YSZ is $11 \times 10^{-6}/^{o}C$[41], it is expected that Si film will be compressed by the YSZ layer. However, this is opposite to the result in Fig. 8, which shows almost the same stress in Si/YSZ/glass and Si/glass. Therefore, we infer that the tensile stress in Fig. 8 may be caused by the densification during the phase transition from amorphous to crystalline. This is because the mass density of a-Si containing voids and defects is generally lower than that of crystalline Si[42, 43]. Since Si atoms at the interface are tightly bonded to the underlayer atoms, the Si position may be almost fixed or negligibly changed even after subsequent

pulse irradiation. However, after crystallization, Si atoms over the interface in the bulk of the film move from their original position in the as-deposition state, which may lead to the densification or shrinkage of the Si film. Therefore, this densification causes tensile stress in the crystallized Si film. On the basis of this hypothesis, we can explain the behavior of the stress in Fig. 8 as follows. The c-Si peak position gradually shifts to lower values with X_c up to ~ 40% or $E \leq 70$ mJ/cm^2. This may be in a transition state of densification, in which small crystallized Si regions that had been isolated from one another with amorphous regions make contact with and bind tightly to one another. With further increase in X_c to 80% or in E to ~100 mJ/cm^2, the peak position remains almost constant or unchanged, which means that the strength of the stress or the bonding of Si atoms in the crystallized region is in a steady state. However, with increasing X_c beyond 80% or E beyond 100 mJ/cm^2, the annealed Si films become nearly melted in solid or melted. Then, the lattice alignment of Si atoms occurs and the stress is partially relaxed or released.

Comparison of the FWHM curve with the peak position curve reveals that they seem to be related to each other. When X_c is smaller than 40%, the crystalline quality shown by FWHM is relatively good but is gradually degraded with increasing X_c, and the film stress is not so large but gradually increases with X_c. This is probably because, in the smaller range of X_c, the amount of amorphous phase remains large such that it could relax stress, acting like a sponge. Furthermore the defective crystallization region is small owing to the small E. However, X_c or E increases, since the amorphous region reduces in size and the defective crystallization region extends with X_c. In the midrange of X_c, the FWHM and stress are almost constant because the amorphous network region may change into a crystalline network, including defects and isolated or non-network atomic regions. Atoms constituting

the defects and non-network atomic regions rarely move into the lattice sites at an E lower than the critical melting. However, at X_c of more than 80%, i.e., near or higher than the critical E, some Si atoms in the defect and non-network regions can bond well with other atoms so that FWHM and film stress can be reduced.

4. Discussion

First, we discuss the difference in optical absorption between Si films of Si/YSZ/glass and Si/glass in order to explain the result in Fig. 4. Figure 9 shows the YSZ film thickness (d) dependences of the optical absorptivities A of a-Si and poly-Si films, which are calculated using a fundamental optics theory. The calculation model of the sample structure is drawn schematically in the inset of Fig. 9, in accordance with the actual experimental conditions. In this model, we consider multireflection in a Si film and a YSZ layer in a normal incidence case. The refractive indices of a-Si, poly-Si, YSZ, and the glass substrate are $n_{a-Si} \approx 4.53-i0.897$, $n_{poly-Si} \approx 4.15-i0.0428$, $n_{YSZ} \approx 2.18$, and $n_{SiO_2} \approx 1.46$, respectively, at a wavelength of 532 nm[44, 45]. It can be seen that the absorptivity of the a-Si film in a 60 nm a-Si/glass structure (d = 0), $A \approx 0.546$, is higher than that in a 60 nm a-Si/YSZ/glass structure with d = 60 nm, $A \approx 0.445$. For a poly-Si film, a similar result occurs, but with much smaller values, i.e., $A \approx 0.075$ and $A \approx 0.042$ for d = 0 and d = 60 nm, respectively. This indicates that the Si film in Si/glass is heated more than that in Si/YSZ/glass. This essentially results from the smaller difference in refractive index between Si (n_{Si}) and YSZ (n_{YSZ}) than between Si (n_{Si}) and glass (n_{SiO_2}).

Considering the above differences, the data for Si/YSZ/glass in Fig. 4 are redrawn by the broken blue line, as mentioned earlier. The value of 18.5% is calculated using $A \approx 0.546$ for a-Si/glass and $A \approx 0.445$ for a-Si/YSZ/glass. We can see that the corrected line for

Si/YSZ/glass becomes more fitting to the red line curve for Si/glass in the low-E region. In the high-E or high-X_c region, the poly-Si refractive index should be considered as well as the a-Si refractive index because some regions of irradiated Si films change from an amorphous phase to a polycrystalline phase. Therefore, it can be concluded that the difference in X_c at the same E between Si/YSZ/glass and Si/glass is mainly attributed to the difference in optical absorption between them. Actually, in order to explain the behavior shown in Fig. 4 in more detail, we should take the temperature dependence of the refractive index into account. Owing to this, the absorptivity of poly-Si increases with temperature monotonically, and thus the Si film should be exposed to more heating than that predicted from the calculated absorptivity in Fig. 9[46].

From the aforementioned experimental results and discussion, we speculate a mechanism of Si film crystallization with/without the YSZ CI layer at low and high energy densities E. The schematic models are shown in Fig. 10. At a low energy density in Fig. 10(a) (e.g., $E \approx 29 - 31$ mJ/cm^2 in Fig. 7), in the initial state (e.g., $N \leq 50$ in Fig. 7), nucleation sites may be formed mainly at the interface between Si and the underlayer in both Si/glass and Si/YSZ/glass. According to previous reports on other research studies[47, 48], nucleation in a-Si films occurs faster at the interface than in the bulk. In Si/glass, owing to the lack of crystallographic information on glass, crystallization growth proceeds randomly as does random nucleation. In the Si/YSZ/glass case, in contrast, owing to YSZ being highly oriented or fiber-textured (Fig. 2), the nucleation might be induced more uniformly like a sheet at the interface of the YSZ layer. For example, at $X_c \approx 0$ for $N = 50$ in Fig. 7, there is no observable crystallized region grown from the nucleation. This is probably because the optical absorptivity is smaller than that of Si/glass, as shown in Fig. 9. With increasing

annealing time or pulse number (e.g., $N > 50$), crystallization occurs from the interface and proceeds at a low rate, as shown in Fig. 10(a). The orientation of the crystallized regions might be similar to that of the grains of the YSZ layer, as shown in the right-hand panels in Fig. 10(a), in contrast to the random nucleation and crystallization growth of Si/glass. With increasing N, film bulk nucleation may occur in not only Si/glass but also Si/YSZ/glass, although the crystallized region extends more from the interface, where the nucleation density in the bulk for Si/YSZ/glass is smaller than for Si/glass because of the smaller optical absorptivity. On the other hand, at high E in Fig. 10(b) (e.g., $E > 90$ mJ/cm^2), since the crystallization rate is very high, nucleation and growth occur quickly even with a short annealing time or a small pulse number (e.g., $N \approx 10$). Owing to the higher nucleus density and the lack of crystallographic information in the bulk, crystallization growth from the interface is impeded by bulk random growth and terminates midway in not only Si/glass but also Si/YSZ/glass.

From the above discussion, we expect that annealing with low E will produce Si films with better crystallinity. However, the crystallization rate is so low that it should take a long time for complete crystallization. Annealing with high E can reduce the annealing time, but the crystallized Si films quality becomes poorer or more defective owing to faster random nucleation and crystallization growth.

5. Conclusions

We crystallized Si films on glass substrates with and without a YSZ CI layer in the solid phase by PLA, and investigated their properties mainly by Raman spectroscopy. We obtained the following results. The crystalline fraction X_c increased with the energy density E monotonically in both Si/YSZ/glass and Si/glass. It was found that the crystallization rate

to E was lower for Si/YSZ/glass than for Si/glass. This is because the optical absorption in the Si film for Si/YSZ/glass is lower than that for Si/glass owing to the difference in refractive index between n_{YSZ} and n_{SiO_2}. At the same X_c, the FWHM of the c-Si peak for Si/YSZ/glass was smaller than that for Si/glass, which indicates better crystalline quality of the Si film on the YSZ layer than of that on the glass substrate. It can be considered from this result that Si atoms in Si/YSZ/glass are arranged more orderly during the phase amorphous to crystalline transition and that the defect density is lower in Si/YSZ/glass than in Si/glass. This may be due to the crystallization-induction effect of the YSZ layer. The film stress was tensile and increased with X_c, and almost saturated at approximately X_c = 40%, regardless of using a YSZ layer or not. This can be explained by the mass density change from the amorphous phase to the crystalline phase. From the pulse number N dependences of X_c and FWHM, it was found that, at a small E, X_c increased proportionally with N, but, at a high E, X_c rapidly increased to a near-saturation level with a smaller N. From this result, it can be considered that since a higher E induces a faster random nucleation not only at the interface but also in the bulk in Si films, a smaller E is more suitable for controlling nucleation sites. Therefore, in the CI layer method using a small E, it is possible to control nucleation sites on the YSZ interface to make crystallization growth proceed to the film surface smoothly without random nucleation. However, since it takes a longer time for the complete crystallization of the entire a-Si film, this method is not practical for mass production. We should consider a better method of producing good-quality Si films within a shorter time.

References

[1] X. Duan, C. Niu, V. Sahi, J. Chen, J.-W. Parce, S. Empedocles, and J.-L. Goldman, Nature **425**, 274 (2003).

[2] H. Wang, Int. J. Photoenergy **2011**, ID 801292 (2011).

[3] I.-S. Mulla, N.-S. Ramgir, Y.-K. Hwang, and J.-S. Chang, J. Ind. Eng. Chem. **10**, 1242 (2004).

[4] E. Yablonovitch, E. Kapon, T. J. Gmitter, C. P. Yun, and R. Bhat, IEEE Photonics Technol. Lett. **1**, 41 (1989).

[5] P. F. Carcia, R. S. McLean, M. H. Reilly, and G. Nunes, Jr., Appl. Phys. Lett. **82**, 1117 (2003).

[6] K. Nomura, H. Ohta, K. Ueda, T. Kamiya, M. Hirano, and H. Hosono, Science **300**, 1269 (2003).

[7] K. Nomura, H. Ohta, A. Takagi, T. Kamiya, M. Hirano, and H. Hosono, Nature **432**, 488 (2004).

[8] C. D. Dimitrakopoulos and P. R. L. Malenfant, Adv. Mater. **14**, 99 (2002).

[9] H. Y. Choi, S. H. Kim, and J. Jang, Adv. Mater. **16**, 732 (2004).

[10] T. Sameshima, S. Usui, and M. Sekiya, IEEE Electron Device Lett. **7**, 276 (1986).

[11] S. Uchikoga and N. Ibaraki, Thin Solid Films **383**, 19 (2001).

[12] C. Ipri and G. Kaganowicz, IEEE Trans. Electron Devices **35**, 708 (1988).

[13] G. Liu and S. J. Fonash, Appl. Phys. Lett. **55**, 660 (1989).

[14] R. Kakkad, J. Smith, W. S. Lau, S. J. Fonash, and R. Kerns, J. Appl. Phys. **65**, 2069 (1989).

[15] L. Haji, P. Joubert, J. Stoemenos, and N. A. Economou, J. Appl. Phys. **75**, 3944 (1994).

[16] J. N. Lee, Y. W. Choi, B. J. Lee, and B. T. Ahn, J. Appl. Phys. **82**, 2918 (1997).

[17] S. F. Gong, H. T. G. Hentzell, A. E. Robertsson, L. Hultman, S. E. Hörnström, and G. Radnoczi, J. Appl. Phys. **62**, 3726 (1987).

[18] G. Radnoczi, A. Robertsson, H. T. G. Hentzell, S. F. Gong, and M. A. Hasan, J. Appl. Phys. **69**, 6394 (1991).

[19] S. Y. Yoon, K. H. Kim, C. O. Kim, J. Y. Oh, and J. Jang, J. Appl. Phys. **82**, 5865 (1997).

[20] Z. Jin, G. A. Bhat, M. Yeung, H. S. Kwok, and M. Wong, J. Appl. Phys. **84**, 194 (1998).

[21] S.-W. Lee, Y.-C. Jeon, and S.-K. Joo, Appl. Phys. Lett. **66**, 1671 (1995).

[22] S.-I. Jun, Y.-H. Yang, J.-B. Lee, and D.-K. Choi, Appl. Phys. Lett. **75**, 2235 (1999).

[23] M. Wong, Z. Jin, G. A. Bhat, P. C. Wong, and H. S. Kwok, IEEE Trans. Electron Devices **47**, 1061 (2000).

[24] C.-Y. Hou and Y. S. Wu, Jpn. J. Appl. Phys. **44**, 7327 (2005).

[25] J. C. C. Fan and H. J. Zeiger, J. Appl. Phys. **27**, 224 (1975).

[26] T. Sameshima, M. Hara, and S. Usui, Jpn. J. Appl. Phys. **28**, L2131 (1989).

[27] S. Higashi, N. Ando, K. Kamisako, and T. Sameshima, Jpn. J. Appl. Phys. **40**, 731 (2001).

[28] S.-G. Ryu, I. Gruber, C. P. Grigoropoulos, D. Poulikakos, and S.-J. Moon, Thin Solid Films **520**, 6724 (2012).

[29] J. S. Im and H. A. Atwater, Appl. Phys. Lett. **57**, 1766 (1990).

[30] P. Reinig, F. Fenske, W. Fuhs, A. Schöpke, and B. Selle, Appl. Surf. Sci. **210**, 301 (2003).

[31] S. Hana and S. Horita, Appl. Phys. Express **2**, 041201 (2009).

[32] S. Horita and S. Hana, Jpn. J. Appl. Phys. **49**, 105801 (2010).

[33] S. Hana and S. Horita, Thin Solid Films **517**, 5830 (2009).

[34] S. Ray, S. Mukhopadhyay, T. Jana, and R. Carius, J. Non-Cryst. Solids **299–302**, 761 (2002).

[35] S. Horita, K. Kanazawa, K. Nishioka, K. Higashimine, and M. Koyano, Mater. Res. Soc. Symp. Proc. Vol. **910**, 2006, p. 577.

[36] K. Kitahara, K. Suga, A. Hara, and K. Nakajima, Jpn. J. Appl. Phys. **35**, L1473 (1996).

[37] K. Kitahara, Y. Ohashi, Y. Katoh, A. Hara, and N. Sasaki, J. Appl. Phys. **95**, 7850 (2004).

[38] K. N. Tu, J. W. Mayer, and L. C. Feldman, *Electronic Thin Film Science for Electrical Engineers and Materials Scientists* (Macmillan, New York, 1992), p. 256.

[39] S. M. Sze, *Physics of Semiconductor Devices* (Wiley, New York, 1969) 2nd ed., p. 851.

[40] P. Lengsfeld, N. H. Nickel, C. Genzel, and W. Fuhs, J. Appl. Phys. **91**, 9128 (2002).

[41] S.-C. Hwang, H.-G. Lee, and H.-S. Shin, Korean J. Chem. Eng. **15**(3), 243 (1998).

[42] H. Kumomi and T. Yonehara, J. Appl. Phys. **75**, 2884 (1994).

[43] A. K. Kalkan and S. J. Fonash, Mat. Res. Soc. Symp. Proc. Vol. **558**, 2000, p. 225.

[44] D. Edwards, in *Handbook of Optical Constants of Solids*, ed. E. Palik (Academic Press, New York, 1985) pp. 564, 578.

[45] S. Heiroth, R. Ghisleni, T. Lippert, J. Michler, and A. Wokaun, Acta Materialia **59**, 2330 (2011).

[46] S. Horita, H. Kaki, and K. Nishioka, Jpn. J. Appl. Phys. **46**, 3527 (2007).

[47] L. Haji, P. Joubert, M. Guendouz, N. Duhamel, and B. Loisel, Mat. Res. Soc. Symp. Proc. Vol. **230**, 1992, p. 177.

[48] J. N. Lee, B. J. Lee, D. G. Moon, and B. T. Ah,: Jpn. J. Appl. Phys. **36**, 6862 (1997).

Figure captions

Fig. 1. (Color online) Schematic illustration of laser annealing system.

Fig. 2. (Color online) XRD and RHEED patterns of the 60-nm-thick YSZ layer deposited on the quartz substrate.

Fig. 3. (Color online) Raman spectra of the Si films deposited on the YSZ/glass and glass substrates at energy densities E of (a) 29 – 31 and (b) 104 – 106 mJ/cm^2 with N = 300. Dotted lines in (b) are decomposed components of the three TO mode peaks, one LO mode peak, one LA mode peak, and three peaks due to the glass substrate in a Raman spectrum for Si/YSZ/glass, as an example of deconvolution.

Fig. 4. (Color online) Dependence of crystalline fraction X_c on the laser energy density E with N = 300. The broken line is a curve redrawn with corrected E for Si/YSZ/glass. The correction is mentioned in Sect. 4.

Fig. 5. (Color online) Dependences of (a) microcrystalline fraction X_μ and (b) FWHM of c-Si peak on the laser energy density E with N = 300.

Fig. 6. (Color online) SEM images of the crystallized Si films on (a) glass and (b) YSZ/glass at E = 60 − 80 mJ/cm^2 with N = 300.

Fig. 7. (Color online) Dependences of (a) crystalline fraction X_c and (b) c-Si peak FWHM on the pulse number N. Energy density is the parameter.

Fig. 8. (Color online) Dependences of FWHM and position of c-Si peak on the crystalline fraction X_c for N = 300.

Fig. 9. (Color online) Dependences of absorptivity in Si on the YSZ film thickness d for 60 nm a-Si/YSZ/glass and 60 nm poly-Si/YSZ/glass structures.

Fig. 10. (Color online) Schematic models of crystallization mechanism of Si films with/without YSZ CI layers at (a) low and (b) high energy densities.

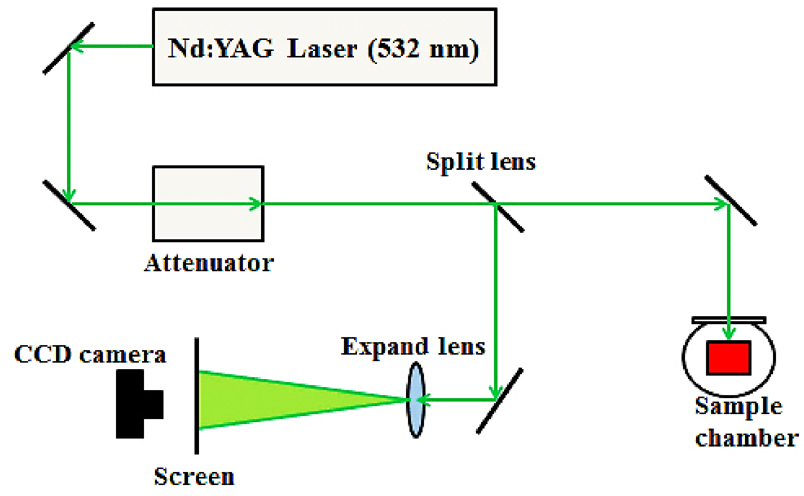

Fig. 1. Mai Thi Kieu Lien and Susumu Horita

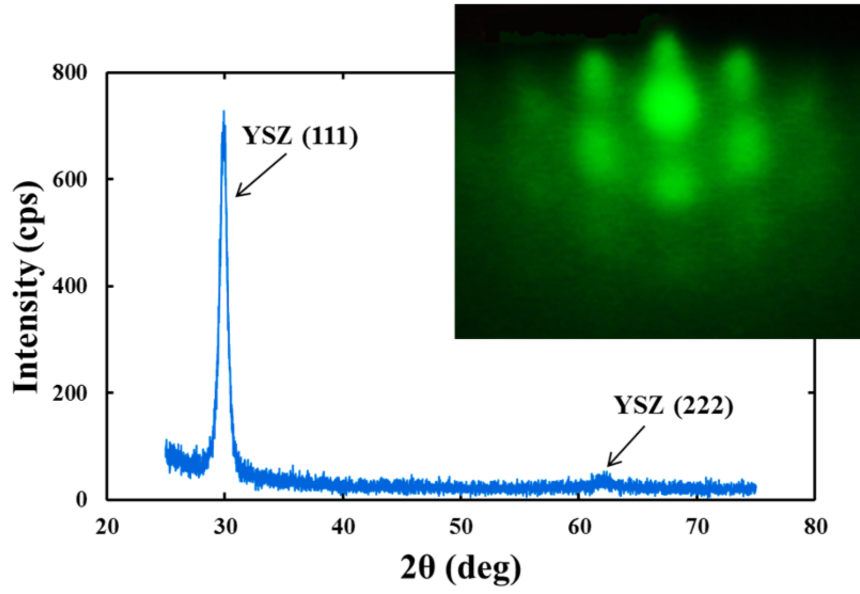

Fig. 2. Mai Thi Kieu Lien and Susumu Horita

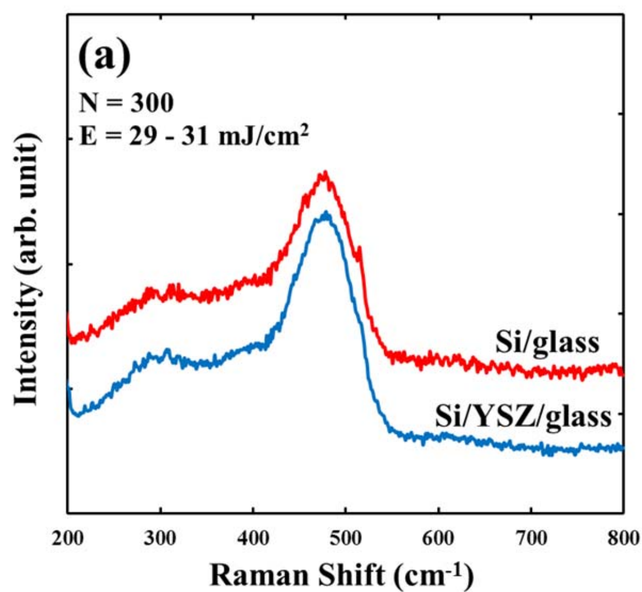

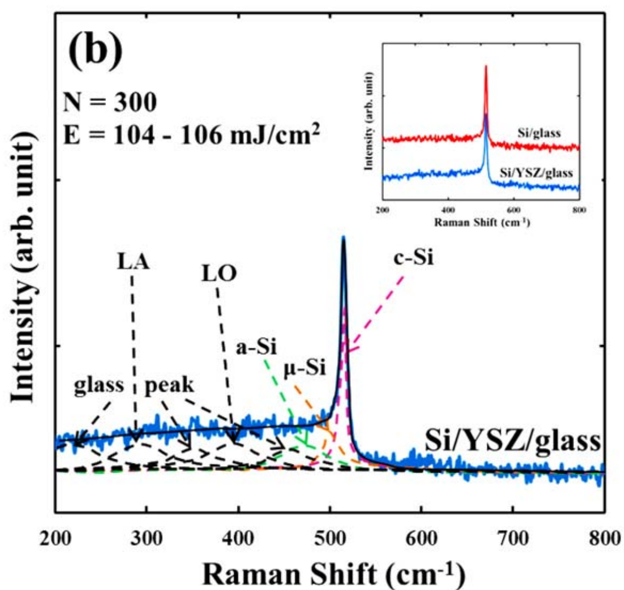

Fig. 3. Mai Thi Kieu Lien and Susumu Horita

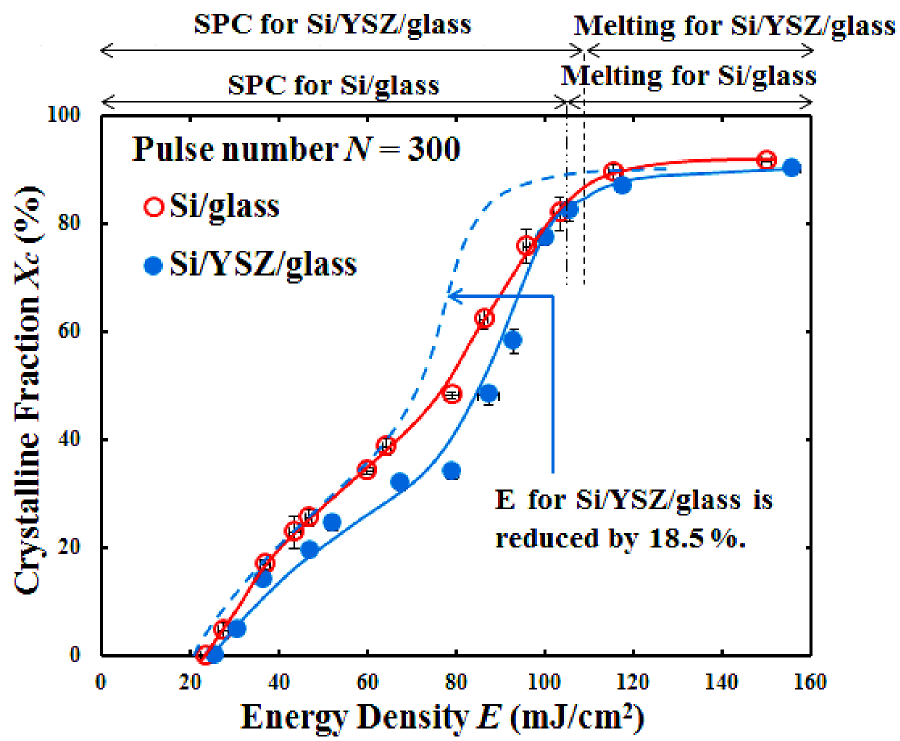

Fig. 4. Mai Thi Kieu Lien and Susumu Horita

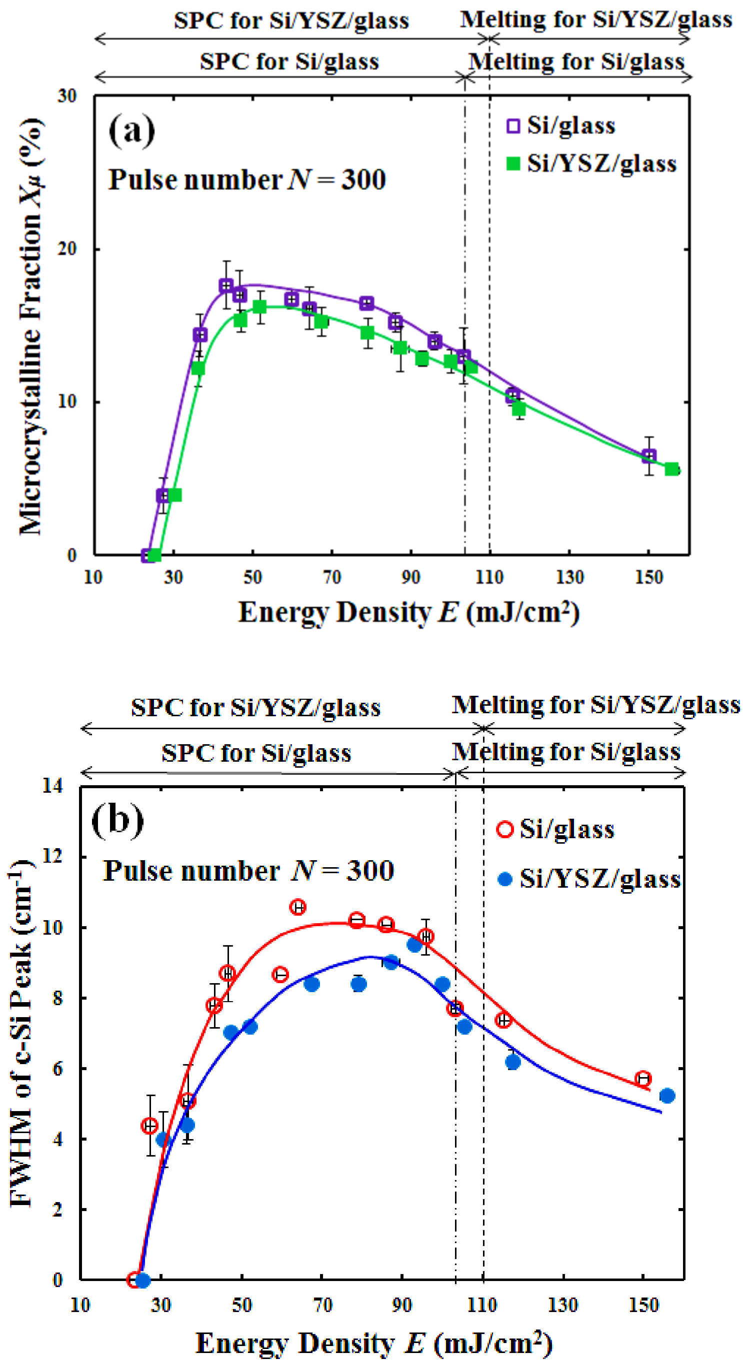

Fig. 5. Mai Thi Kieu Lien and Susumu Horita

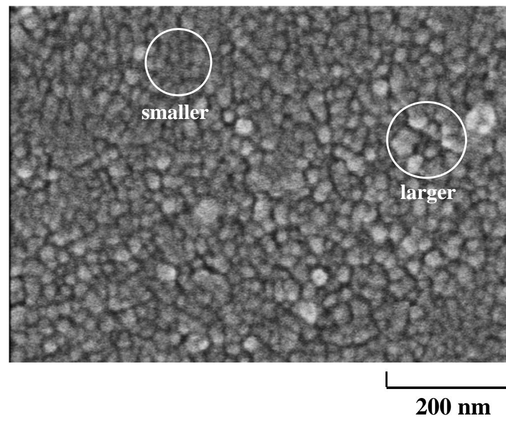

(a) Si/glass

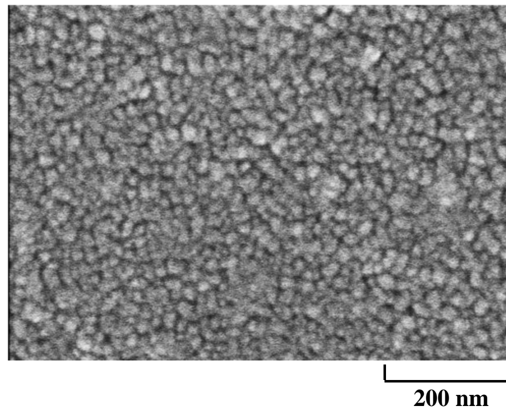

(b) Si/YSZ/glass

Fig. 6. Mai Thi Kieu Lien and Susumu Horita

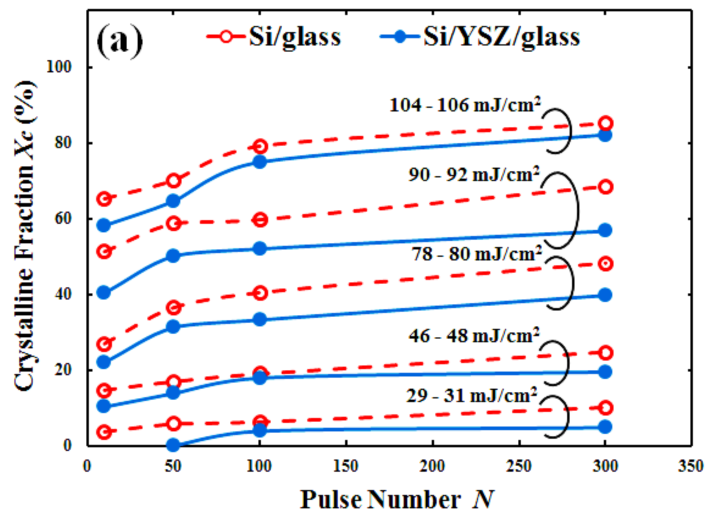

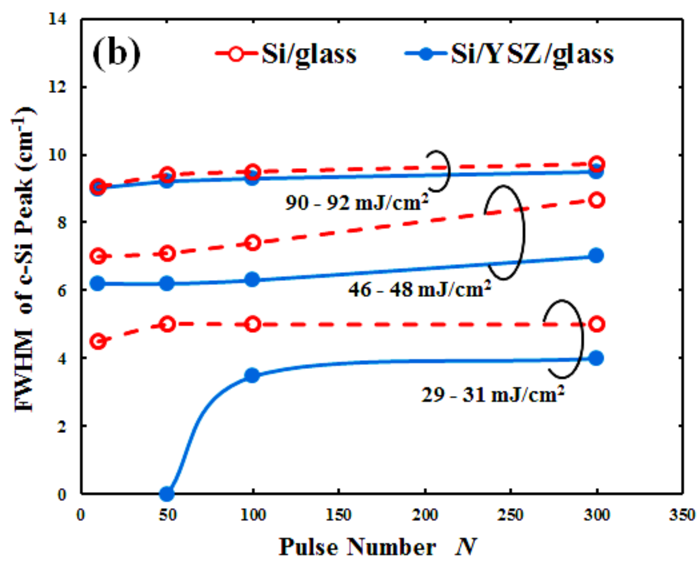

Fig. 7. Mai Thi Kieu Lien and Susumu Horita

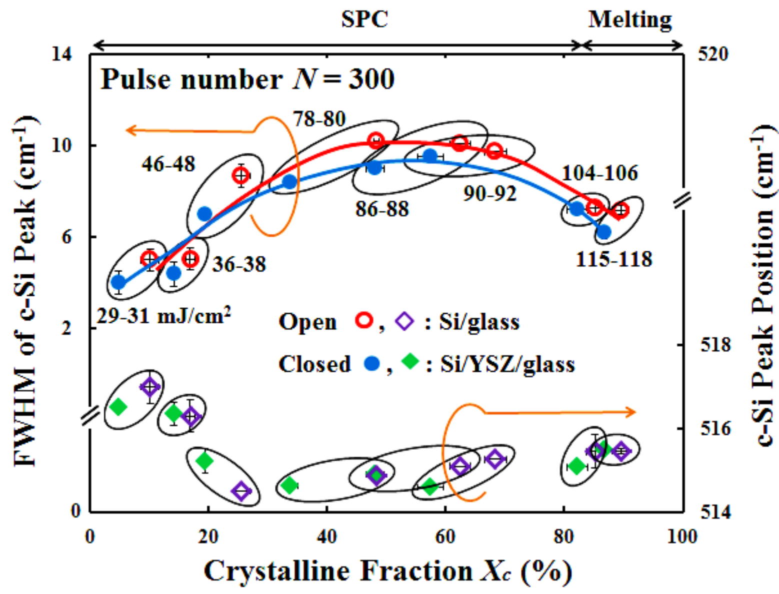

Fig. 8. Mai Thi Kieu Lien and Susumu Horita

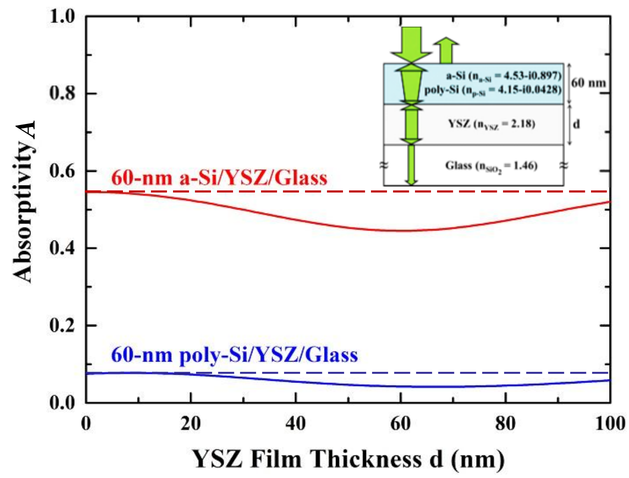

Fig. 9. Mai Thi Kieu Lien and Susumu Horita

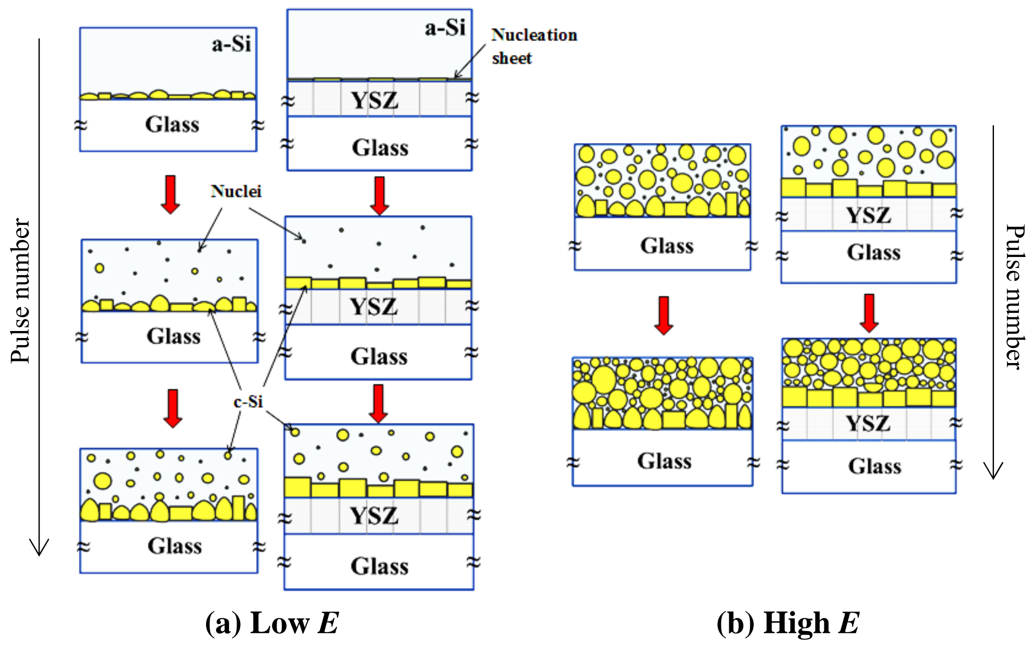

Fig. 10. Mai Thi Kieu Lien and Susumu Horita